

Adsorption-Controlled Epitaxy and Twin Control of γ -GaSe on GaAs (111)B

Joshua Eickhoff,^{1,2} Wendy L. Sarney,² Sina Najmaei,² Daniel A. Rhodes,^{1,3} and Jason Kawasaki^{1,3}

¹*University of Wisconsin–Madison, Department of Materials Science and Engineering*

²*U.S. Army DEVCOM Army Research Laboratory, Adelphi, MD 20783*

³*University of Wisconsin–Madison, Department of Physics*

(Dated: March 10, 2026)

The III-Se layered semiconductors, including InSe and GaSe, are promising optoelectronic materials due to their relatively high electron mobilities at room temperature, nonlinear optical responses, ferroelectricity, self-passivated van der Waals surfaces, and ability to alloy and synthesize heterostructures for bandgap engineering. Adsorption control is a widely utilized strategy for controlling the stoichiometry and phase formation of these materials; however, the bounds of the adsorption-controlled growth window for GaSe have not been systematically established. Additionally, challenges with control over polytype and twinning remain. Here, we use molecular beam epitaxy to experimentally map the adsorption-controlled growth window of GaSe films on vicinal GaAs (111)B substrates. The observed phase boundaries show qualitative agreement with Ellingham diagram predictions. All films crystallize in the γ ($R3m$) polytype. Increasing growth and annealing temperature leads to decreased mosaicity measured by x-ray rocking curve and smoother surfaces measured by atomic force microscopy, at the expense of a transition from singly oriented γ to twinned γ with 60° rotated domains.

I. INTRODUCTION

The III-Se post transition metal monochalcogenides (e.g., GaSe, InSe, and their alloys) host attractive properties for optoelectronic and spintronic applications, including a thickness tuned parabolic to M-shaped dispersion of the valence bands [1, 2], van der Waals interfaces that relax the lattice matching constraints for heteroepitaxy [3], and the ability to engineer band gaps through alloying [4] or synthesis of heterostructures [3]. These materials crystallize in tetralayer Se-III-III-Se blocks separated by van der Waals gaps, where differences in tetralayer-tetralayer stacking registry define the different polytypes. Compared to transition metal dichalcogenides (e.g., MoSe₂, WSe₂, MoS₂) that contain low vapor pressure refractory metals like Mo or W, the higher vapor pressure of group III metals makes the III-Se materials more amenable to large-area scalable synthesis by physical vapor deposition techniques, including molecular beam epitaxy (MBE) [5–9]. However, key synthesis challenges for these materials remain, including stoichiometry control, polytype control, and suppression of twinning.

While adsorption-control is often implicitly utilized to control the stoichiometry of III-Se films during MBE growth [5–9], for GaSe the bounds of this window and its thermodynamic basis have not been systematically established. Adsorption control, the synthesis of a line compound that is in equilibrium with a volatile constituent, is widely utilized in MBE growth [10–15]. The canonical example is GaAs, which has self-limited stoichiometry over a wide range of arsenic overpressure [10, 11]. This self-regulated stoichiometry, and the associated point defect concentrations below parts per billion, has enabled world record electron mobilities in MBE-grown GaAs [16, 17] with applications for high electron mobility transistors, lasers [18], and quantum sciences [19]. A recent study

mapped the stability of the line compound InSe versus volatile Se and competing In-Se phases [20]; a similar relationship is expected for GaSe but has not yet been systematically mapped and compared to theory.

A second challenge is control of polytypes and twinning. GaSe crystallizes in β (2R), ϵ (2H), γ (3R), γ' (3R), and δ (4H) polytypes [6–8, 21–25] (Appendix Figure 5), each with similar formation energies [7, 26]. The most commonly observed polytype for MBE grown GaSe is γ ($R3m$), which typically forms 60° rotated twins [7, 21, 23, 24]. Controlling twins is essential for electronic and optoelectronic devices because twin boundaries can act as non-radiative recombination centers [27] and can substantially scatter electrons, reducing carrier mobilities [28].

Here, we experimentally map the adsorption-controlled growth window for GaSe films by MBE on GaAs (111)B substrates. The observed phase boundaries qualitatively agree with the thermodynamic prediction from an Ellingham diagram. We find that growth temperature produces a tradeoff of crystal quality metrics: lower temperature growth produces simply oriented γ with rough surfaces and broad X-ray rocking curve widths, whereas high temperature improves the roughness and rocking curve width at the expense of forming 60° twins. We speculate that overcoming kinetic barriers may be responsible for twinning at high temperatures.

II. METHODS

GaSe films were grown in a homemade chalcogenide MBE system. GaSe films were grown on epi-ready GaAs (111)B with a 4° miscut towards $\langle 110 \rangle$ (AXT). The in-plane lattice parameters of $a_{GaSe} = 3.74 \text{ \AA}$ and $a_{GaAs,110} = 3.995 \text{ \AA}$ correspond to a -6.5% mismatch. Substrates were indium bonded to sample plates and

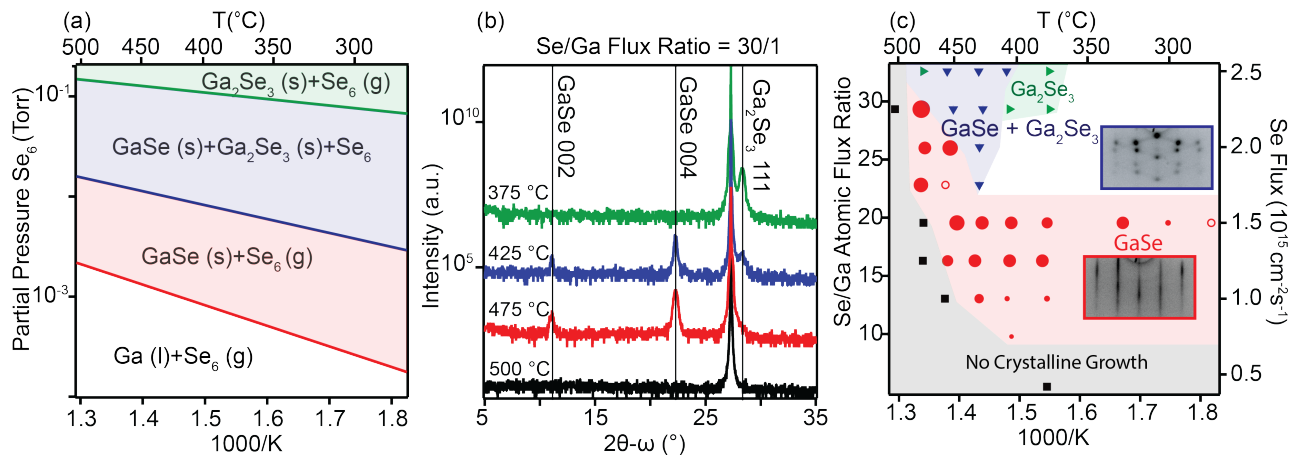


FIG. 1. (a) Ellingham diagram for the Ga-Se calculated using Se_6 as the gaseous species. (b) Symmetric $2\theta-\omega$ x-ray diffraction scans for films grown at a Se/Ga atomic flux ratio of 30 for varying growth temperatures. (c) Experimentally observed phases for MBE growth of GaSe on GaAs (111)B. Inserts show Reflection High Energy Electron Diffraction (RHEED) patterns for GaSe and mixed GaSe + Ga_2Se_3 . Filled marker size corresponds to the inverse of the GaSe 004 ω rocking curve full width at half maximum ($1/\Delta\omega_{\text{fwhm}}$), which scales from $1/1.172^\circ$ to $1/4.506^\circ$. Open marker indicates no rocking curve measured.

pumped in a high vacuum (10^{-8} Torr) loadlock before loading into the growth chamber. In the MBE chamber, substrates were heated to 580°C with a Se flux of $\sim 10^{15}$ atoms/ cm^2s for 20 minutes to desorb surface oxides, as monitored by the reflection high energy electron diffraction (RHEED). Sample temperatures were then decreased to $300 - 500^\circ\text{C}$ for GaSe film growth. Sample temperatures were measured using a thermocouple that was calibrated to the native oxide desorption temperature of GaAs and to the melting point of indium.

GaSe films with a nominal thickness of 45 nm were grown via co-deposition using a standard effusion cell for Ga (9.99999%) and a hot lipped effusion cell for Se (99.999%). The hot lip is operated at 250°C to produce a mixture of Se_2 , Se_5 , Se_6 , and Se_7 , where the resulting Se flux is primarily Se_6 [29]. The Ga flux was fixed at 7.67×10^{13} atoms/ cm^2s , while the Se flux was varied from 5×10^{14} to 2.5×10^{15} atoms/ cm^2s . Effusion cell fluxes were measured using a quartz crystal microbalance calibrated by Rutherford Backscattering Spectrometry.

Several GaSe films were annealed up to 520°C after film growth to increase the atomic scale ordering. Previous studies demonstrate that while the Ga-Se sticking coefficients are vanishingly small for film growth above 500°C [7, 30, 31], GaSe films can be annealed to higher temperatures after growth using appropriately matched Ga and Se fluxes to compensate for film desorption from the surface. To perform these anneals, we first grew GaSe at 400°C and then shuttered the Ga. The sample temperature was then increased to 520°C at a rate of $20^\circ\text{C}/\text{min}$. Subsequently, both Se and Ga shutters were opened and the sample was held at 520°C for an additional 30 minutes. Then both shutters were closed and the samples were cooled to room temperature at a rate of $20^\circ\text{C}/\text{min}$ in a residual background of Se [31]. X-ray reflectivity (XRR) measurements (Appendix Figure 6)

show that this anneal procedure results in a thickness change from 43 nm before the anneal to 48 nm after the anneal.

$2\theta-\omega$ survey scans, ω rocking curves, and in-plane azimuthal φ scans were measured using a Panalytical Empyrean X-ray diffractometer using $\text{Cu K}\alpha$ radiation with a 4 bounce Ge 220 monochromator on the incident side. No monochromator was used on the analyzer side. AFM images were acquired in tapping mode using an Asylum Cypher S atomic force microscope (Asylum Research/Oxford Instruments, USA) with a silicon tapping mode cantilever (AC160TSA R3; Olympus/Asylum Research).

Cross-sectional TEM samples were prepared with a Thermo Scientific Helios G4 UX Dualbeam focused ion beam (FIB) system. Selected area diffraction patterns (SAED, aperture size $20 \mu\text{m}$) and high angle annular dark field (HAADF) images were collected from an aberration-corrected JEOL ARM 200F scanning transmission electron microscope (STEM) operated at 200 keV. Based on the dimensions of the electron transparent regions of the TEM specimens, the SAED patterns typically probed a total area of $40 \mu\text{m}^2$ which includes both GaSe film and GaAs substrate. We use linear transformations to align the selected area diffraction patterns to crystallographic directions and convert from camera pixel spacing to physical units of Q . These transformations included brightness scaling, translation, rotation, and linear x, y scaling, aligning to the GaAs substrate $22\bar{4}$ reflections. In Appendix Figure 8 we show an example of this rescaling for the film grown at 400°C . Simulated x-ray diffraction patterns were computed using CrystalMaker SingleCrystal based on β , δ , γ , and ϵ -GaSe structure files from the Inorganic Crystal Structure Database (ICSD) [32–36]. For γ' , which does not appear in ICSD, we use the atomic positions reported in Ref. [7].

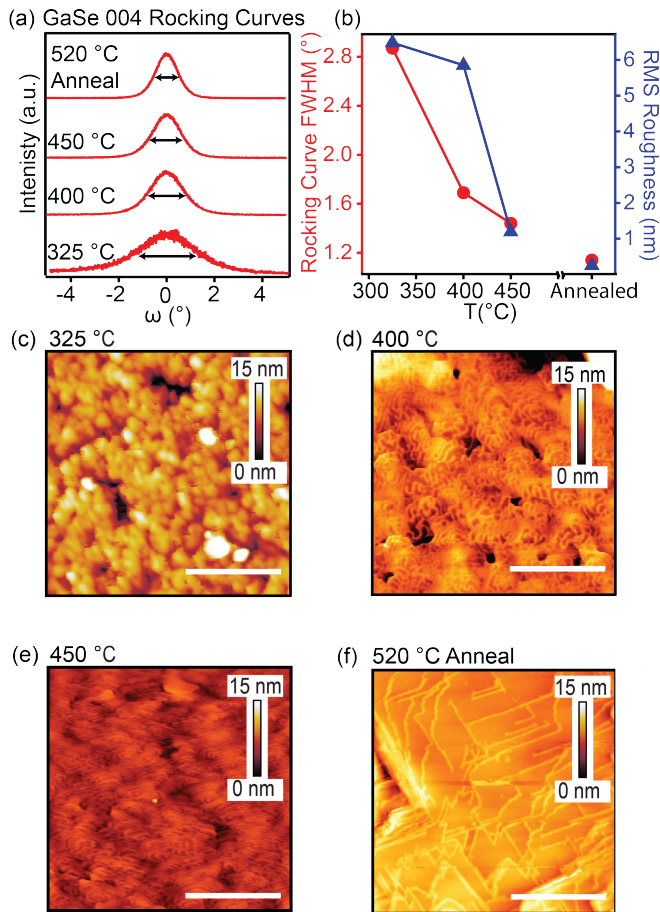


FIG. 2. (a) X-ray rocking curves of the GaSe 004 reflection for fixed Se/Ga flux ratio 20/1. (b) Summarized rocking curve width and root mean square (RMS) roughness versus growth or anneal temperature. (c-f) Atomic Force Microscopy (AFM) topography images of GaSe samples grown at 325 °C, 400 °C, 450 °C, and 400 °C plus a post growth anneal at 520 °C. Scale bars are 400 nm.

III. RESULTS AND DISCUSSION

To guide synthesis we begin by computing the Ellingham diagram, which describes the bulk thermodynamic stability of Ga-Se phases as a function of temperature, T , and Se partial pressure. Note this should be considered a qualitative rather than quantitative guide, since the bulk equilibrium Ellingham diagram does not consider contributions from surface energies, strain, and kinetic factors. We construct this diagram based on tabulated bulk thermodynamic data [37–41]. For simplicity we compute the diagram for Se_6 , which is the primary volatile species expected from our hot lipped Se effusion cell operated at 250 °C [42]. In Appendix Figure 7, we compare with a similar calculation for Se_2 .

In Fig. 1(a), the red shaded region bounded between the red and blue lines defines the expected adsorption-controlled growth window for GaSe. In between these

lines, solid GaSe exists in equilibrium with Se vapor, and since GaSe is a line compound its stoichiometry is self-limited. The lower red line is derived from the Gibbs free energy for the GaSe decomposition reaction $\text{GaSe}(s) \Leftrightarrow \text{Ga}(l) + \frac{1}{6} \text{Se}_6(g)$. Below this curve, solid GaSe decomposes into liquid Ga and vapor Se. The blue curve is defined by the reaction $\text{Ga}_2\text{Se}_3 \Leftrightarrow 2 \text{Ga}(l) + \frac{1}{2} \text{Se}_6(g)$. Above this line, Ga_2Se_3 becomes stable along with GaSe, leading to a region where both GaSe and Ga_2Se_3 are stable (blue region). The green line is defined by the reaction $4\text{GaSe}(s) + \text{Se}_6(g) \Leftrightarrow 2\text{Ga}_2\text{Se}_3(s) + 2\text{Se}_2(g)$. Pure Ga_2Se_3 and Se vapor exist above this line.

To experimentally validate this prediction, we synthesize films by MBE on intentionally 4° miscut, As-terminated GaAs (111)B substrates over a range of growth temperatures and relative Se fluxes (Methods). Figs 1(b,c) present representative reflection high energy electron diffraction (RHEED) patterns and symmetric $2\theta - \omega$ x-ray diffraction (XRD) measurements of GaSe films. For decreasing growth temperature at fixed Se/Ga flux, we observe an evolution from no crystalline growth (black curve), to phase pure GaSe (red), to GaSe mixed with Ga_2Se_3 (blue), to pure phase Ga_2Se_3 (green). We summarize the XRD-determined phases as a function of growth temperature and Se/Ga atomic flux ratio in Fig. 1(d), where we find qualitative agreement with the phases expected from the Ellingham diagram.

Increasing the growth temperature improves the standard crystal quality metrics, include a narrowing of the GaSe 004 x-ray rocking curves indicating decreased mosaicity (Fig. 2(a,b)), and a reduced surface roughness as measured by AFM (Fig. 2(b,c-f)). These trends are in qualitative agreement with previous studies [7], although the observed rocking curve widths are broader than previous reports. GaSe growth on a smoothed GaAs buffer layer, rather than direct growth on de-oxidized GaAs (111)B, may be a route to decrease the mosaicity and further smoothen the resulting GaSe film surface. Buffer layers are a commonly used strategy for smoothening III-V and other surfaces for homoepitaxy [43] and heteroepitaxy [44] with reduced dislocation densities.

Note that for Se fluxes up to 2.25×10^{15} atoms/cm²s, GaSe film growth above a growth temperature of 475 °C leads to a sharp decrease of the Ga and Se sticking coefficients, and no crystalline growth is observed (Fig. 1(b,c) black curve). To access higher temperatures for improved atomic scale ordering, we employ a growth plus anneal approach, previously used by Ref. [31], where we first grow a film at 400 °C where the sticking coefficient of GaSe is close to unity, then shutter the Ga and anneal the GaSe film at 520 °C under a combined $\text{Se}_x + \text{Ga}$ flux to balance against the rate of GaSe decomposition. We find that this high temperature anneal sharpens the x-ray rocking curve width and decreases the RMS surface roughness (Fig. 2(b)). Minimal change in thickness was confirmed by XRR, indicating the observed improvements are structurally driven and not thickness-dependent.

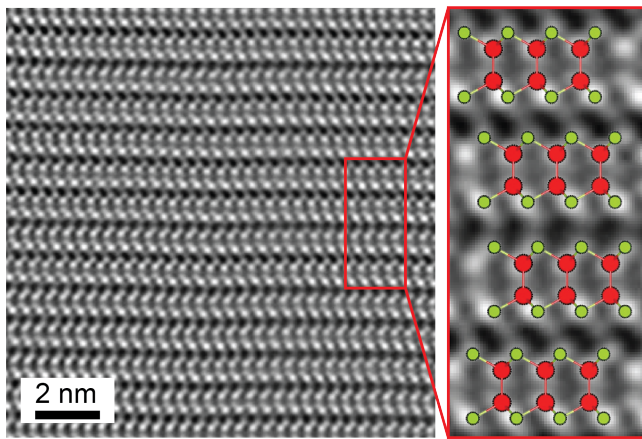


FIG. 3. HAADF-STEM image of the GaSe film grown at 400 °C and annealed at 520 °C, measured along a $\langle 100 \rangle_{\text{GaSe}} \parallel \langle 110 \rangle_{\text{GaAs}}$ zone axis. Ga atoms are in red, and the Se atoms are in light green.

Since it is difficult to distinguish the different GaSe polytypes and twinning by $00L$ -type reflections alone, we use real space imaging by HAADF-STEM and off axis reflections by SAED and x-ray azimuthal scans. Figure 3 shows a HAADF-STEM image of the film grown at 400 °C and annealed at 520 °C. The $ABC - ABC$ stacking with “C” shaped Se-Ga-Ga-Se tetralayers corresponds to the γ polytype, and within this $\sim 180 \text{ nm}^2$ field of view only a single orientation of γ is imaged.

Selected area electron diffraction in the TEM, surveyed over a larger area ($40 \mu\text{m}^2$), indicate this annealed sample has R0 and R60 rotated γ twin variants (Fig. 4(c)). Here, twinning appears as double spots, since rhombohedral γ ($R3m$) has 3-fold rather than 6-fold rotation around the c axis. In Appendix Figure 10 we show that twinned γ is the most consistent identification compared to the other potential polytypes. X-ray diffraction azimuthal φ scans over macroscopic areas (few mm^2) display an apparent 6-fold symmetry of the γ $10\bar{1}0$ (Fig. 4(f), red curve), which arises from the superposition of R0 and R60 domains each with 3-fold rotation.

Interestingly, we find that while samples grown or annealed at $T \geq 450 \text{ °C}$ are twinned, the sample grown at 400 °C is singly oriented. This is observed both in the SAED of the 400 °C sample, which appears as single rather than double spots (Fig. 4(a)), and in the azimuthal x-ray scan, which shows 3-fold rather than 6-fold rotation (Fig. 4(f), blue). We speculate that the appearance of singly-oriented γ at lower growth temperature (400 °C), compared to twinned γ at higher growth temperature (450 °C), arises due to thermal activation of mobile adatoms or ad-closers over kinetic barriers at high temperature.

The effect of post growth annealing implies a slightly different mechanism. For the annealed film, presumably the initial GaSe growth at 400 °C produced singly oriented γ , and it is the act of annealing to 520 °C that

produced twins. This suggests a solid-solid phase transition/reorientation of an already formed GaSe film, rather than differences in mobility of surface adatoms during film growth. Further studies are required in order to fully understand this 60 degree reorientation.

IV. CONCLUSION

In summary, we mapped the adsorption-controlled MBE growth window for GaSe films on GaAs (111)B substrates and found a qualitative agreement with predictions from the Ellingham diagram. Increasing the growth temperature decreases the mosaicity and surface roughness, in agreement with previous reports. However, whereas the high temperature growth and annealing produce twinned γ polytype, lower temperature growth at 400 °C produces singly oriented γ . Thus, there is a compromise of desirable GaSe film metrics as a function of growth temperature. Further studies with more careful surface preparation, including smoothed GaAs buffer layers and well defined step edges, may be required to understand and better control twinning in MBE-grown GaSe films.

V. ACKNOWLEDGMENTS

J.E. acknowledges support from the DEVCOM Army Research Laboratory (ARL) Research Associateship Program (RAP), administered by Oak Ridge Associated Universities (ORAU) for ARL through Cooperative Agreement (CA) W911NFT22T2T0097.

Additional support for MBE growth facilities (J.E. and J.K.K.) was provided by the NSF QLCI HQAN (NSF award No. 2016136). D.A.R. acknowledges additional support from the Office of Naval Research (N000142512276).

We acknowledge the use of facilities and instrumentation in the Wisconsin Center for Nanoscale Technology. This Center is partially supported by the Wisconsin Materials Research Science and Engineering Center (NSF DMR-2309000) and by the University of Wisconsin–Madison.

VI. AUTHOR DECLARATIONS

A. Conflict of interest

The authors have no conflicts to disclose.

VII. DATA AVAILABILITY

Raw data corresponding to each figure are made available at doi:xx to be finalized upon acceptance.

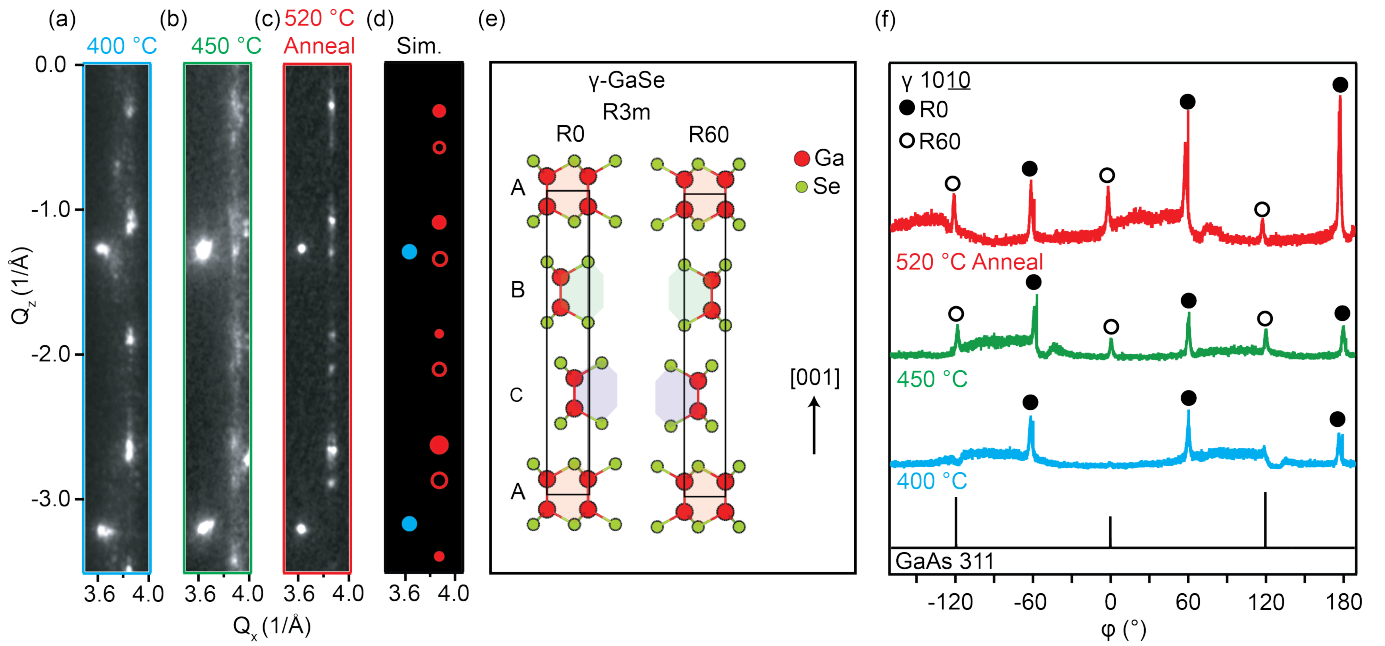


FIG. 4. (a-c) Selected area electron diffraction (SAED) of the $20L$ -type reflections for films grown at 400 °C and 450 °C, and the film annealed at 520 °C. Full SAED patterns in Appendix Figure 9. (d) Simulated electron diffraction pattern. (e) Crystal structure of γ -GaSe for the R0 and R30 twin orientations, viewed along $\langle 100 \rangle_{\text{GaSe}}$ and $\langle 110 \rangle_{\text{GaSe}}$, respectively. (f) Azimuthal φ x-ray diffraction scans of the GaSe $10\bar{1}0$ film reflection, referenced to the GaAs substrate 311 reflection.

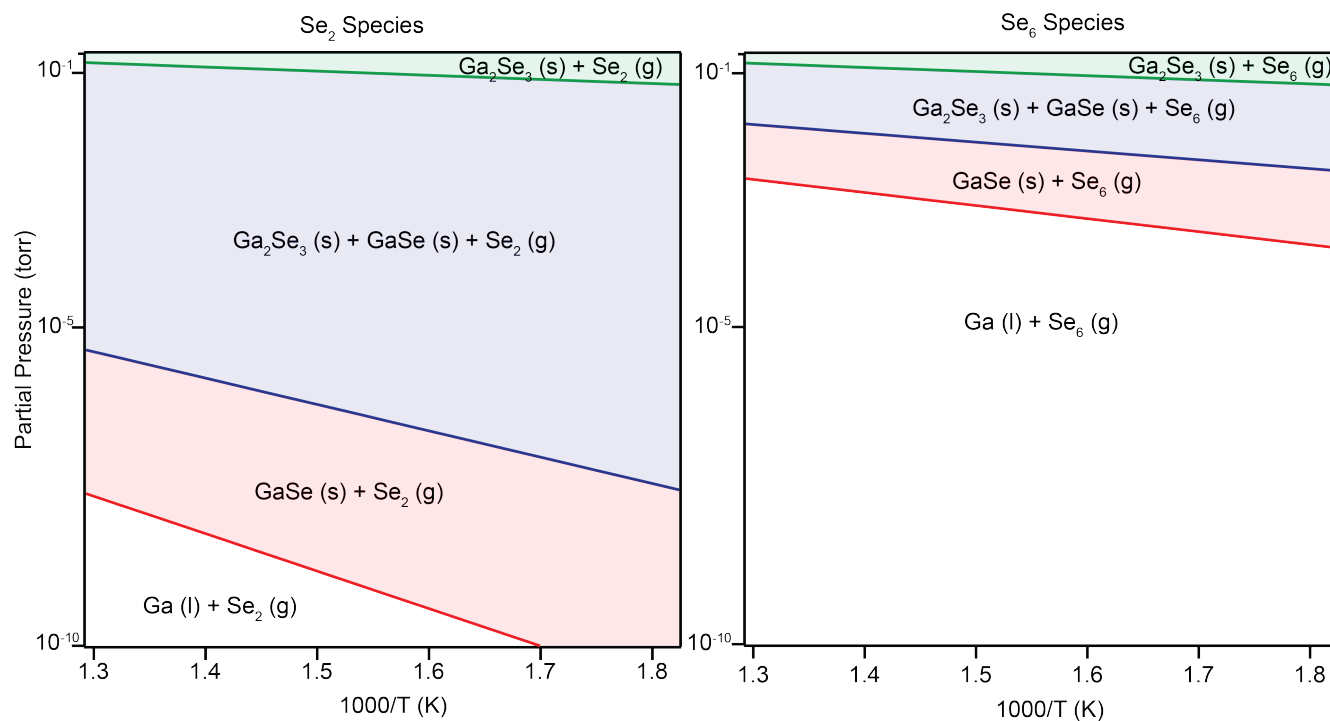


FIG. 7. Ellingham diagrams comparing Se₂ versus Se₆ as the gaseous species. [37–41]

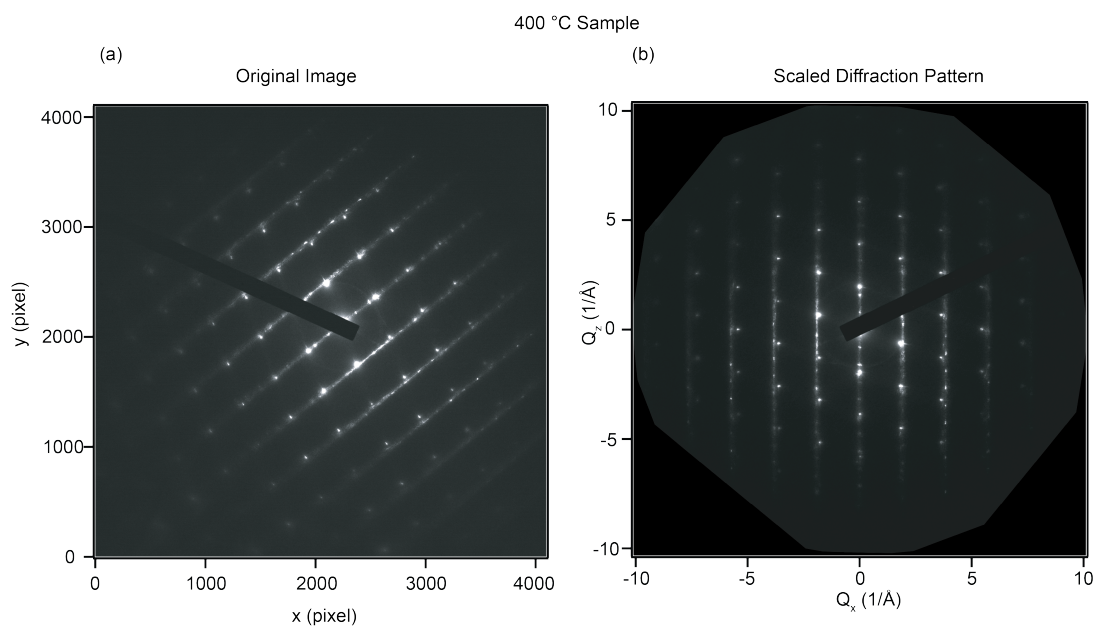


FIG. 8. (a) Original SAED image for the 400 °C sample (b) Scaled diffraction pattern

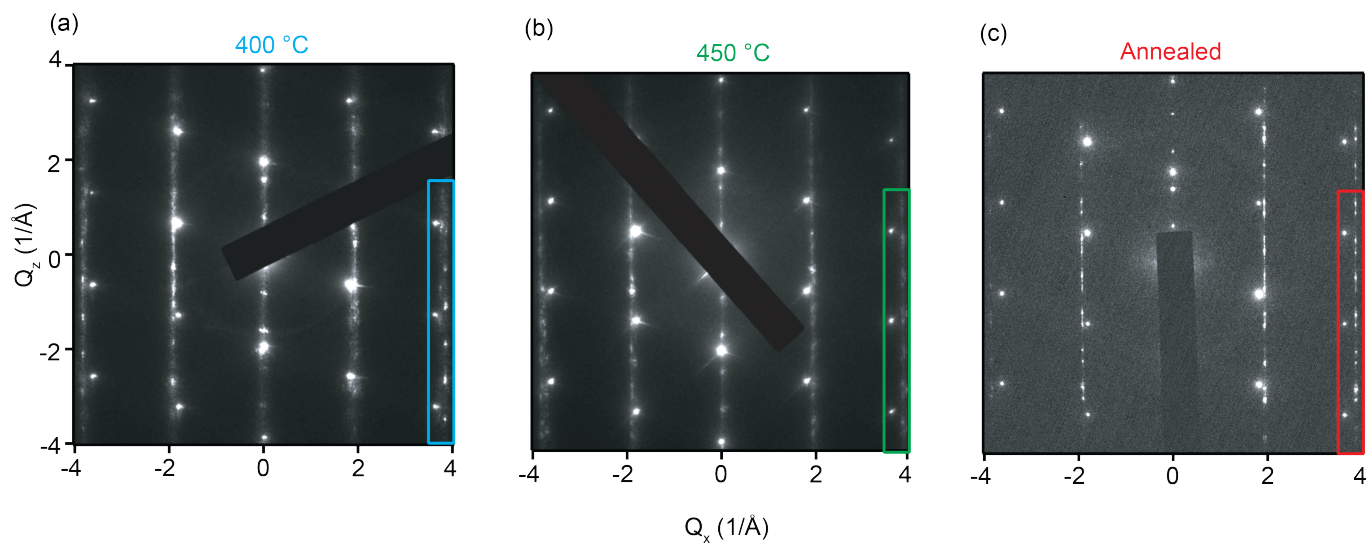


FIG. 9. Electron diffraction patterns for (a) 400 °C, (b) 450 °C, and (c) 520 °C anneal samples. Boxes indicate locations of intensity line cuts.

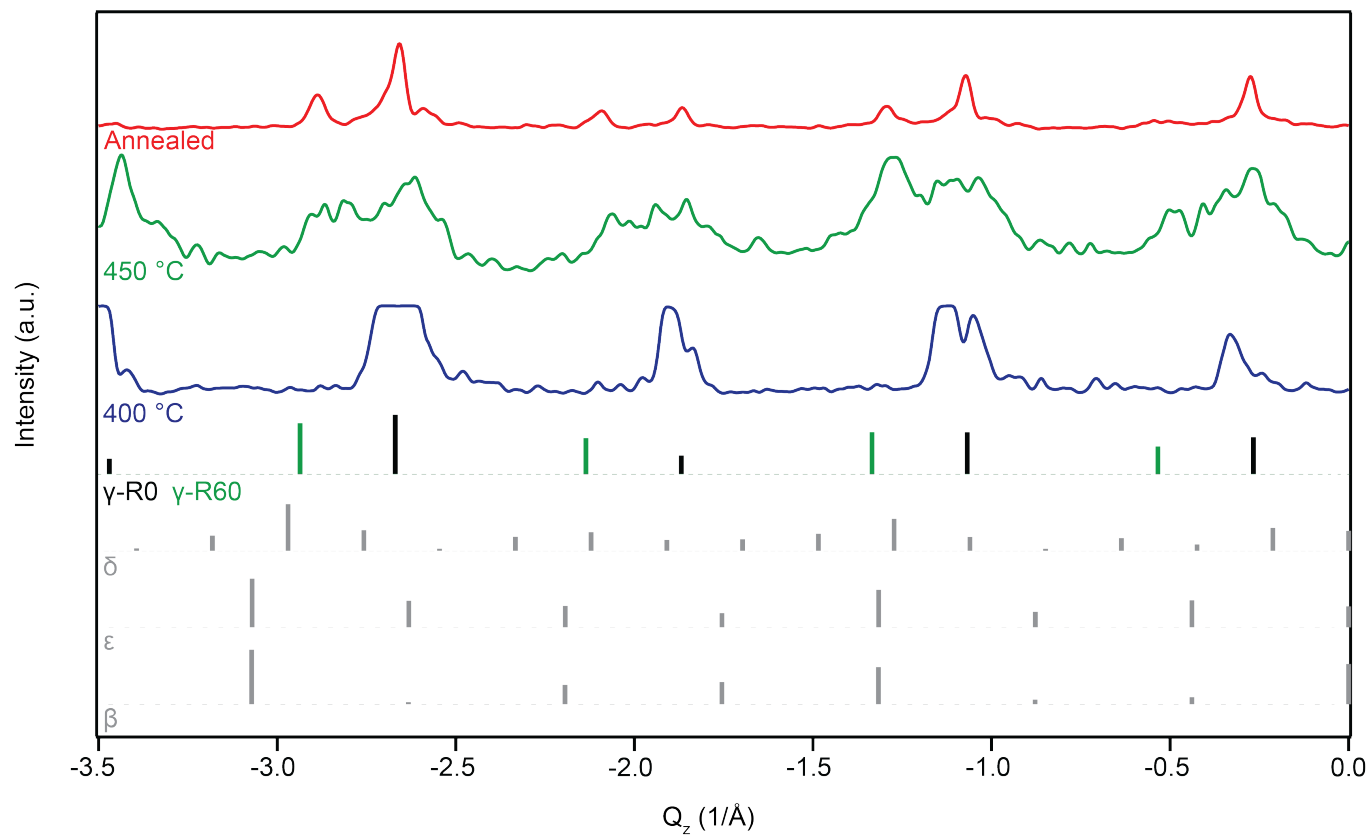


FIG. 10. Intensity linecuts of the SAED at $H = 2$, compared to simulated electron diffraction patterns for the different polytypes.

- [1] Chan Su Jung, Fazel Shojaei, Kidong Park, Jin Young Oh, Hyung Soon Im, Dong Myung Jang, Jeunghee Park, and Hong Seok Kang. Red-to-ultraviolet emission tuning of two-dimensional gallium sulfide/selenide. *ACS Nano*, 9(10):9585–9593, 2015. doi:10.1021/acsnano.5b04876. URL <https://doi.org/10.1021/acsnano.5b04876>.
- [2] Arne Budweg, Dinesh Yadav, Alexander Grupp, Alfred Leitenstorfer, Maxim Trushin, Fabian Pauly, and Daniele Brida. Control of excitonic absorption by thickness variation in few-layer gase. *Phys. Rev. B*, 100:045404, Jul 2019. doi:10.1103/PhysRevB.100.045404. URL <https://link.aps.org/doi/10.1103/PhysRevB.100.045404>.
- [3] Marcel S. Claro, Juan P. Martínez-Pastor, Alejandro Molina-Sánchez, Khalil El Hajraoui, Justyna Grzonka, Hamid Pashaei Adl, David Fuertes Marrón, Paulo J. Ferreira, Oleksandr Bondarchuk, and Sascha Sadewasser. Van der waals heteroepitaxy of gase and inse, quantum wells, and superlattices. *Advanced Functional Materials*, 33(13):2211871, 2023. doi:<https://doi.org/10.1002/adfm.202211871>. URL <https://advanced.onlinelibrary.wiley.com/doi/abs/10.1002/adfm.202211871>.
- [4] Quynh Trang Tran, Thi Bich Tuyen Huynh, Tu Huynh Pham, Umeshwar Reddy Nallasani, Hong-Jyun Wang, Nhu Quynh Diep, Wu-Ching Chou, Van-Quy Le, Kung-Hwa Wei, and Thanh Tra Vu. Molecular beam epitaxy of mixed dimensional ingase/gase hybrid heterostructures on c-sapphire. *ACS Applied Electronic Materials*, 6(10):7448–7455, 2024.
- [5] Nobuaki Kojima, Kei Sato, Akira Yamada, Makoto Konagai, and Kiyoshi Takahashi Kiyoshi Takahashi. Epitaxial growth of gase films by molecular beam epitaxy on gaas (111),(001) and (112) substrates. *Japanese journal of applied physics*, 33(10B):L1482, 1994.
- [6] Choong Hee Lee, Sriram Krishnamoorthy, Dante J. O’Hara, Mark R. Brenner, Jared M. Johnson, John S. Jamison, Roberto C. Myers, Roland K. Kawakami, Jinwoo Hwang, and Siddharth Rajan. Molecular beam epitaxy of 2d-layered gallium selenide on gan substrates. *Journal of Applied Physics*, 121(9):094302, 03 2017. doi:10.1063/1.4977697. URL <https://doi.org/10.1063/1.4977697>.
- [7] Mingyu Yu, Sahani Amaya Iddawela, Jiayang Wang, Maria Hilse, Jessica L. Thompson, Danielle Reifsnnyder Hickey, Susan B. Sinnott, and Stephanie Law. Quasi-van der waals epitaxial growth of gamma’-gase nanometer-thick films on gaas(111)b substrates. *ACS Nano*, 18(26):17185–17196, 2024. doi:10.1021/acsnano.4c04194. URL <https://doi.org/10.1021/acsnano.4c04194>. PMID: 38870462.
- [8] N Jedrecy, R Pinchaux, and M Eddrief. Epitaxy of layered compounds: Gase on si (111). *Physical Review B*, 56(15):9583, 1997.
- [9] M Eddrief, C Sébenne, A Sacuto, M Balkanski, et al. Heteroepitaxy of gase layered semiconductor compound on si (111) 7×7 substrate: a van der waals epitaxy? *Journal of crystal growth*, 135(1-2):1–10, 1994.
- [10] Al Y Cho and JR Arthur. Molecular beam epitaxy. *Progress in solid state chemistry*, 10:157–191, 1975.
- [11] JR Arthur Jr. Interaction of ga and as2 molecular beams with gaas surfaces. *Journal of Applied Physics*, 39(8):4032–4034, 1968.
- [12] Dongxue Du, Patrick J Strohbeen, Hanjong Paik, Chenyu Zhang, Konrad T Genser, Karin M Rabe, Paul M Voyles, Darrell G Schlom, and Jason K Kawasaki. Control of polymorphism during epitaxial growth of hyperferroelectric candidate liznsb on gasb (111) b. *Journal of Vacuum Science & Technology B*, 38(2), 2020.
- [13] Estiaque H Shourov, Ryan Jacobs, Wyatt A Behn, Zachary J Krebs, Chenyu Zhang, Patrick J Strohbeen, Dongxue Du, Paul M Voyles, Victor W Brar, Dane D Morgan, et al. Semi-adsorption-controlled growth window for half-heusler fevsb epitaxial films. *Physical Review Materials*, 4(7):073401, 2020.
- [14] Bharat Jalan, Pouya Moetakef, and Susanne Stemmer. Molecular beam epitaxy of srtio3 with a growth window. *Applied Physics Letters*, 95(3), 2009.
- [15] JF Ihlefeld, A Kumar, Venkatraman Gopalan, Darrell G Schlom, YB Chen, XQ Pan, Tassilo Heeg, Jurgen Schubert, X Ke, P Schiffer, et al. Adsorption-controlled molecular-beam epitaxial growth of bifeo3. *Applied Physics Letters*, 91(7), 2007.
- [16] Loren Pfeiffer, KW West, HL Stormer, and KW Baldwin. Electron mobilities exceeding 107 cm²/v s in modulation-doped gaas. *Applied Physics Letters*, 55(18):1888–1890, 1989.
- [17] Daniel C Tsui, Horst L Stormer, and Arthur C Gossard. Two-dimensional magnetotransport in the extreme quantum limit. *Physical Review Letters*, 48(22):1559, 1982.
- [18] Justin C Norman, Daehwan Jung, Zeyu Zhang, Yating Wan, Songtao Liu, Chen Shang, Robert W Herrick, Weng W Chow, Arthur C Gossard, and John E Bowers. A review of high-performance quantum dot lasers on silicon. *IEEE Journal of Quantum Electronics*, 55(2):1–11, 2019.
- [19] James Nakamura, Saeed Fallahi, Harshad Sahasrabudhe, Rajib Rahman, Shuang Liang, Geoffrey C Gardner, and Michael J Manfra. Aharonov–bohm interference of fractional quantum hall edge modes. *Nature Physics*, 15(6):563–569, 2019.
- [20] Derrick SH Liu, Maria Hilse, Andrew R Lupini, Joan M Redwing, and Roman Engel-Herbert. Growth of nanometer-thick γ -inse on si (111) 7×7 by molecular beam epitaxy for field-effect transistors and optoelectronic devices. *ACS Applied Nano Materials*, 6(16):15029–15037, 2023.
- [21] Justyna Grzonka, Marcel S Claro, Alejandro Molina-Sánchez, Sascha Sadewasser, and Paulo J Ferreira. Novel polymorph of gase. *Advanced Functional Materials*, 31(48):2104965, 2021.
- [22] Sergei Valer’evich Sorokin, Pavel Sergeevich Avdienko, Irina Vladimirovna Sedova, Demid A Kirilenko, Mariya Aleksandrovna Yagovkina, Aleksandr Nikolaevich Smirnov, V Yu Davydov, and Sergei Viktorovich Ivanov. Molecular-beam epitaxy of two-dimensional gase layers on gaas (001) and gaas (112) substrates: structural and optical properties. *Semiconductors*, 53(8):1131–1137, 2019. doi:<https://doi.org/10.1134/S1063782619080189>.
- [23] Mustaqeem Shiffa, Benjamin T Dewes, Jonathan Bradford, Nathan D Cottam, Tin S Cheng, Christopher J Mellor, Oleg Makarovskiy, Kazi Rahman, James N O’Shea, Peter H Beton, et al. Wafer-scale two-dimensional semi-

- conductors for deep uv sensing. *Small*, 20(7):2305865, 2024.
- [24] Takahiro Yonezawa, Tatsuya Murakami, Koichi Higashimine, Antoine Fleurence, Yoshifumi Oshima, and Yukiko Yamada-Takamura. Atomistic study of gase/ge (111) interface formed through van der waals epitaxy. *Surface and Interface Analysis*, 51(1):95–99, 2019.
- [25] Nhu Quynh Diep, Cheng-Wei Liu, Ssu-Kuan Wu, Wu-Ching Chou, Sa Hoang Huynh, and Edward Yi Chang. Screw-dislocation-driven growth mode in two dimensional gase on gaas (001) substrates grown by molecular beam epitaxy. *Scientific reports*, 9(1):17781, 2019.
- [26] Jichen Dong, Leining Zhang, Xinyue Dai, and Feng Ding. The epitaxy of 2d materials growth. *Nature Communications*, 2020. doi:10.1038/s41467-020-19752-3.
- [27] Sobin Mathew, Vladislav Kurtash, Bernd Hahnlein, Pavithra Manoharan, Mithun Krishna, Heiko O Jacobs, and Jorg Pezoldt. Grains, grain boundaries in single and few layer mos2. *Nano Express*, 6, 2025. doi:10.1088/2632-959X/ade9e4.
- [28] Jejune Park, Kan-Hao Xue, Mireille Mouis, Francois Triozon, and Alessandro Cresti. Electron transport properties of mirror twin grain boundaries in molybdenum disulfide: Impact of disorder. *Physical Review B*, 100(23):235403, 2019.
- [29] H Cheng, JM DePuydt, MA Haase, and JE Potts. Molecular-beam epitaxy growth of znse using a cracked selenium source. *Journal of Vacuum Science & Technology B: Microelectronics Processing and Phenomena*, 8(2):181–186, 1990.
- [30] Mingyu Yu, Lottie Murray, Matthew Doty, and Stephanie Law. Epitaxial growth of atomically thin ga2se2 films on c-plane sapphire substrates. *Journal of Vacuum Science & Technology A*, 41(3):032704, 04 2023. ISSN 0734-2101. doi:10.1116/6.0002446. URL <https://doi.org/10.1116/6.0002446>.
- [31] Mnig-Wei Chen, HoKwon Kim, Dmitry Ovchinnikov, Agnieszka Kuc, Thomas Heine, Olivier Renault, and Andras Kis. Large-grain mbe-grown gase on gaas with a mexican hat-like valence band dispersion. *npj 2D Materials and Applications*, 2018. doi:10.1038/s41699-017-0047-x.
- [32] A. Kuhn, R. Chevalier, and A. Rimsky. Atomic structure of a 4H GaSe polytype named δ -type. *Acta Crystallographica Section B*, 31(12):2841–2842, Dec 1975. doi:10.1107/S0567740875009016. URL <https://doi.org/10.1107/S0567740875009016>.
- [33] S. Benazeth, Nguyen-Huy Dung, M. Guittard, and P. Laruelle. Affinement sur monocristal de la structure du polytype 2H du séléniure de gallium GaSe forme β . *Acta Crystallographica Section C*, 44(2):234–236, Feb 1988. doi:10.1107/S0108270187010102. URL <https://doi.org/10.1107/S0108270187010102>.
- [34] K. Cenzual, L. M. Gelato, M. Penzo, and E. Parthé. Inorganic structure types with revised space groups. I. *Acta Crystallographica Section B*, 47(4):433–439, Aug 1991. doi:10.1107/S0108768191000903. URL <https://doi.org/10.1107/S0108768191000903>.
- [35] Konrad Schubert, Erhard Dörre, and Manfred Kluge. Zur kristallehemie der b-metalle iii. kristallstruktur von gase und inte. *International Journal of Materials Research*, 46(3):216–224, 1955. doi:doi:10.1515/ijmr-1955-460312. URL <https://doi.org/10.1515/ijmr-1955-460312>.
- [36] A. W. Stevenson. Thermal vibrations and bonding in GaAs: an extended-face crystal study. *Acta Crystallographica Section A*, 50(5):621–632, Sep 1994. doi:10.1107/S0108767393013947. URL <https://doi.org/10.1107/S0108767393013947>.
- [37] J. Berkowitz and W. A. Chupka. Equilibrium composition of selenium vapor; the thermodynamics of the vaporization of hgse, cdse, and srse. *The Journal of Chemical Physics*, 45(11):4289–4302, 12 1966. ISSN 0021-9606. doi:10.1063/1.1727488. URL <https://doi.org/10.1063/1.1727488>.
- [38] Umesh Gaur, Hua-Cheng Shu, Aspy Mehta, and Bernhard Wunderlich. Heat capacity and other thermodynamic properties of linear macromolecules. i. selenium. *Journal of Physical and Chemical Reference Data*, 10(1):89–118, 01 1981. ISSN 0047-2689. doi:10.1063/1.555642. URL <https://doi.org/10.1063/1.555642>.
- [39] M. Ider, R. Pankajavalli, W. Zhuang, J. Y. Shen, and T. J. Anderson. Thermochemistry of the ga-se system. *ECS Journal of Solid State Science and Technology*, 4(5):Q51, apr 2015. doi:10.1149/2.0011507jss. URL <https://doi.org/10.1149/2.0011507jss>.
- [40] A.V. Tyurin, K.S. Gavrichev, L.N. Golushina and V.E. Gorbunov, and V.P. Zlomanov. Heat capacity and thermodynamic functions of ga2se3 from 14 to 320 k. *Inorganic Materials*, 41(11), 2005.
- [41] David Sedmidubský, Zdeněk Sofer, Štěpán Huber, Jan Luxa, Radek Točík, Tomáš Mahnel, and Květoslav Růžička. Chemical bonding and thermodynamic properties of gallium and indium monochalcogenides. *The Journal of Chemical Thermodynamics*, 128:97–102, 2019. ISSN 0021-9614. doi:<https://doi.org/10.1016/j.jct.2018.08.013>. URL <https://www.sciencedirect.com/science/article/pii/S0021961418305305>.
- [42] R. Yamdagni and R. F. Porter. Mass spectrometric and torsion effusion studies of the evaporation of liquid selenium. *Journal of The Electrochemical Society*, 115(6):601, jun 1968. doi:10.1149/1.2411356. URL <https://doi.org/10.1149/1.2411356>.
- [43] Michael B. Whitwick, T. Tiedje, and Tian Li. Linear smoothing of gaas(100) during epitaxial growth on rough substrates. *Journal of Crystal Growth*, 310(13):3192–3196, 2008. ISSN 0022-0248. doi:<https://doi.org/10.1016/j.jcrysgro.2008.03.019>. URL <https://www.sciencedirect.com/science/article/pii/S0022024808002406>.
- [44] JA Carlin, SA Ringel, EA Fitzgerald, M Bulsara, and BM Keyes. Impact of gaas buffer thickness on electronic quality of gaas grown on graded ge/gesi/si substrates. *Applied Physics Letters*, 76(14):1884–1886, 2000.